Neurons and *β*-Cells of the Pancreas Express Connexin36, Forming Gap Junction Channels that Exhibit Strong Cationic Selectivity

Feliksas F. Bukauskas
Dominick P. Purpura Department of Neuroscience, Albert Einstein College of Medicine, 1300 Morris Park Avenue, Bronx 10461, NY, USA, feliksas.bukauskas@einstein.yu.edu

Abstract

We examined the permeability of connexin36 (Cx36) homotypic gap junction (GJ) channels, expressed in neurons and *β*-cells of the pancreas, to dyes differing in molecular mass and net charge. Experiments were performed in HeLa cells stably expressing Cx36 tagged with EGFP by combining a dual whole-cell voltage clamp and fluorescence imaging. To assess the permeability of the single GJ channel (P_γ), we used a dual-mode excitation of fluorescent dyes that allowed us to measure cell-to-cell dye transfer at levels not resolvable using whole-field excitation solely. We demonstrate that P_γ of Cx36 for cationic dyes (EAM-1$^+$ and EAM-2$^+$) is ~10-fold higher than that for an anionic dye of the same net charge and similar molecular mass, Alexa fluor-350 (AFl-350$^-$). In addition, P_γ for Lucifer yellow (LY^{2-}) is approximately fourfold smaller than that for AFl-350$^-$, which suggests that the higher negativity of LY^{2-} significantly reduces permeability. The P_γ of Cx36 for AFl-350 is approximately 358, 138, 23 and four times smaller than the P_γs of Cx43, Cx40, Cx45, and Cx57, respectively. In contrast, it is 6.5-fold higher than the P_γ of mCx30.2, which exhibits a smaller single-channel conductance. Thus, Cx36 GJs are highly cation-selective and should exhibit relatively low permeability to numerous vital negatively charged metabolites and high permeability to K$^+$, a major charge carrier in cell– cell communication.

Keywords

Intercellular communication; Connexin; Gap junction; Permeability; Voltage gating; Cationic selectivity

Introduction

The connexins (Cxs) are members of a large family of integral membrane proteins that form gap junction (GJ) channels, which provide a pathway for electrical signaling and metabolic communication (Bukauskas and Verselis 2004; Harris 2007). Each GJ channel is formed of two apposed hemichannels (aHCs) representing hexamers/connexons oligomerized in the endoplasmic reticulum (ER)/Golgi complex and inserted in the plasma membrane. Expression of Cxs is tissue- and organ-specific, and many cells express several Cx isoforms, allowing them to form homotypic, heterotypic and/or heteromeric GJ channels (Bukauskas and Verselis 2004). Cx36 is one of three major neuronal Cxs (m30.2/hCx31.9, Cx36, Cx45)

and the sole Cx in β-cells of the pancreas in adults (Condorelli et al. 1998; Serre-Beinier et al. 2000).

Cx-based GJs differ in single-channel conductance, perm selectivity and voltage gating (Goldberg et al. 2004; Harris 2007; Rackauskas et al. 2007a; Palacios-Prado and Bukauskas 2009; Heyman et al. 2009; Veenstra et al. 1995). Each aHC has two gating mechanisms, both sensitive to transjunctional voltage (V_j), the *fast* gate and the *slow* (or *loop*) gate (Bukauskas and Verselis 2004). In addition, GJ channels can be gated by intracellular H^+, Ca^{2+}, posttranslational modifications and a variety of chemical agents (Harris 2001). The mechanisms by which these factors exert their effect on GJs remain unclear, although H^+ and Ca^{2+} ions may both act through the *slow* gate (Peracchia 2004). GJs respond to V_j with decay of junctional conductance (g_j) to a steady state ($g_{j,ss}$) or a minimal conductance (Bennett and Verselis 1992). This property has been explained by single-channel studies showing that GJ channels close with fast transitions from the main open state with conductance, γ_{open}, to a subcon-ducting or residual conductance state, γ_{res}, which is a property of the *fast* gate (Bukauskas and Weingart 1994; Bukauskas and Peracchia 1997). Sensitivity to V_j is Cx type–specific, and Cx36 is one of the least V_j-sensitive Cxs among the 21 members of this family. Typically, homo-typic GJs show a maximum g_j at $V_j = 0$ mV and a symmetric $g_{j,ss} - V_j$ dependence, which is due to the presence of two gates in each hemichannel (Harris 2001). Fast and slow V_j-sensitive gating mechanisms have been reported in GJ channels formed of different Cx isoforms (reviewed in Bukauskas and Verselis 2004) as well as in unapposed/nonjunctional Cx46 hemichannels (Trexler et al. 1996).

It is well established that GJs are permeable to second messengers, such as Ca^{2+}, cAMP and IP_3, in a Cx type-dependent manner (Hernandez et al. 2007; Bedner et al. 2006; Ponsioen et al. 2007). For example, Cx43 GJs demonstrate ~ 15-fold higher permeability than Cx32 GJs for glutamate, glutathione, ADP and AMP and ~ 10-fold lesser permeability to adenosine (Goldberg et al. 2004). All of the aforementioned molecules are comparable in molecular mass and net charge to the fluorescent dyes used in this study. Cx isoforms exhibit different permeability (P_j) to the same compound, which for some Cxs can differ 1,000-fold (Rackauskas et al. 2007b). Single-channel permeability (P_γ) is not necessarily proportional to single-channel conductance or pore diameter (Goldberg et al. 2004; Rackauskas et al. 2007b). In addition, the fast V_j-sensitive gating mechanism operates as a selectivity filter, restricting metabolic cell–cell communication while preserving electrical coupling (Qu and Dahl 2002; Bukauskas et al. 2002a). In primary β-cells only Cx36 forms GJs that exhibit higher permeability to positively charged tracers (Charpantier et al. 2007). Also, it has been shown that β-cells are able to exchange by negatively charged molecules, such as phosphorylated glucose metabolites and nucleotides (reviewed in Jain and Lammert 2009), suggesting that cationic selectivity of Cx36 GJs is not absolute. It is well documented that Cx36-expressing cells exhibit relatively low cell–cell coupling, low single-channel conductance and low sensitivity of V_j gating (Srinivas et al. 1999; Teubner et al. 2000). However, there are no reported data demonstrating Cx36 permeability at the single-channel level for different dyes, which is necessary to quantify charge selectivity and to compare with permse-lectivity of other Cxs. Original reports on the permeability of Cx36 GJs demonstrated some disagreement in regard to Lucifer yellow (LY) (Srinivas et al. 1999; Teubner et al. 2000). Due to difficulties with detection of LY transfer between cells expressing Cx36 in brain slices (Campbell et al. 2011) and retina (Pan et al. 2010), these and many similar studies preferentially used neurobiotin. In contrast, it was shown that electrical synapses between Mauthner cells and the club endings of nerve afferents are permeable to LY (Pereda et al. 1995); Mauthner cells express Cx35, the fish ortholog of Cx36 (Pereda et al. 2003). Thus, it is quite possible that Cx36 is permeable to cations and anions but at significantly different rates.

Here, we examined the permselectivity of homotypic GJs formed of Cx36. We demonstrate that Cx36 exhibits ~10-fold higher permeability to cationic than to anionic dyes of approximately the same molecular mass and net charge. Combined electrophysiological and fluorescence imaging studies allowed us to evaluate the permeability of the single Cx36 GJ channel for different dyes and to compare the permeability of Cx36 with that of other connexins.

Materials and Methods

Cells and Culture Conditions

Experiments were performed on HeLa cells (ATCC CCL2) stably transfected with Cx36 tagged with green fluorescence to the C terminus (Cx36-EGFP). Cells were grown in Dulbecco's modified Eagle medium supplemented with 8 % FBS. All media and culture reagents were obtained from Life Technologies (Bethesda, MD). For simultaneous electrophysiological and fluorescence recording, cells were grown on coverslips and then transferred to an experimental chamber (Bukauskas 2001) mounted on the stage of an inverted Olympus (Tokyo, Japan) IX-70 microscope equipped with a Hamamatsu (Bridgewater, NJ) digital camera and filter wheels housing appropriate excitation and emission filters adapted to image EGFP and the fluorescent dyes used in this study.

Electrophysiological Recordings of Cell–Cell Coupling

Junctional conductance, g_j, was measured in selected cell pairs by a dual whole-cell voltage-clamp method. Cells 1 and 2 of a cell pair were voltage-clamped independently with separate patch-clamp amplifiers (EPC8; HEKA Elektronik, Lambrecht, Germany) at the same holding potential, $V_1 = V_2$. By stepping the voltage in cell 1 and keeping the other constant, junctional current was measured as the change in current in the unstepped cell 2, $I_j = I_2$. Thus, g_j was obtained from the ratio $-I_j/V_j$, where V_j is transjunctional voltage and the negative sign indicates that I_j measured in cell 2 is oppositely oriented to the one measured in cell 1. To minimize the effect of series resistance on measurements of g_j (Wilders and Jongsma 1992), we maintained pipette resistances below 3 MOhm. Patch pipettes were pulled from glass capillary tubes with filaments. Voltages and currents were acquired and analyzed using the MIO-163 A/D converter (National Instruments, Austin, TX) and custom-made software (Trexler et al. 1999). Cells were perfused at room temperature in a modified Krebs-Ringer (MKR) solution containing (in mM) NaCl, 140; KCl, 4; CaCl$_2$, 2; MgCl$_2$, 1; glucose, 5; pyruvate, 2; HEPES, 5 (pH 7.4). Patch pipettes were filled with a solution containing (in mM) KCl, 130; NaAsp, 10; MgCl$_2$, 1; CaCl$_2$, 0.2; EGTA, 2; HEPES, 5 (pH 7.2, $[Ca^{2+}]_i = 5 \times 10^{-8}$ M).

Fluorescence Imaging and Dye Transfer Studies

Fluorescence signals were acquired using an ORCA digital camera (Hamamatsu) with UltraVIEW software for image acquisition and analysis (Perkin Elmer Life Sciences, Boston, MA). For dye transfer studies, a given dye was introduced into cell 1 of a pair through a patch pipette in whole-cell voltage-clamp mode. Typically, this resulted in rapid loading of cell 1, followed by dye transfer to the neighboring cell 2. A whole-cell recording in the dye recipient cell (cell 2) was established ~6–10 min after opening the patch in cell 1. This allowed measurement of g_j and avoided dye leakage into pipette 2 during dye permeability measurements.

Evaluation of GJ permeability of dyes from changes in fluorescence intensity in both cells was previously detailed (Rackauskas et al. 2007b; Palacios-Prado et al. 2009, 2010). In brief, cell-to-cell flux (J_j) of dye in the absence of transjunctional voltage ($V_j = 0$ mV) can

be determined from changes of dye concentration in cell 2 (ΔC_2) over time interval (Δt) as follows:

$$J_i = vol_2(\Delta C_2/\Delta t) \quad (1)$$

where vol_2 is the volume of cell 2. Then, according to the modified (Verselis et al. 1986) Goldman-Hodgkin-Katz (GHK) equation (Hille 2001), the total junctional permeability (P_j) can be described in consequence:

$$P_j = \frac{J_i}{C_1 - C_2} = \frac{vol_2 \cdot (\Delta C_2/\Delta t)}{C_1 - C_2} \quad (2)$$

where C_1 and C_2 are dye concentrations in cell 1 (dye donor) and cell 2 (dye recipient), respectively. Cell volume was approximated as a hemisphere. The diameter of a hemisphere was determined by averaging the longest and shortest diameters of the cell; on average, the volume of examined HeLa cells was ~ 1,800 μm^3. Assuming that dye concentration is directly proportional to fluorescence intensity ($C = k \cdot FI$), then equation 2 can be modified as follows:

$$P_j = \frac{(vol_2 \cdot \Delta FI_2/\Delta t)}{FI_1 - FI_2} \quad (3)$$

where $\Delta FI_2 = FI_{2,n+1} - FI_{2,n}$ is the change in FI in cell 2 over time, $\Delta t = (t_{n+1} - t_n)$; n is the nth time point in the recording.

Most of the fluorescent dyes and reagents were purchased from Invitrogen (Eugene, OR). EAM-1 and EAM-2 cationic dyes (see below) were obtained from Macrocyclics (Dallas, TX). To minimize dye bleaching, studies were performed using time-lapse imaging, which exposed cells to a low-intensity light for ~ 0.5 s every 6 s or more. We also used low dye concentrations in the pipette solution, typically 0.1 mM and below, which minimized phototoxicity but still provided satisfactory fluorescence intensities.

Data Analysis and Statistics

The analysis was performed using SigmaPlot software (Systat, Richmond, CA), and averaged data are reported as means ± SEM.

Results

Cell-to-Cell Dye Transfer Studies

The major goal of this study was to determine the permeability of the Cx36 GJ channel to dyes that differ in molecular mass and net charge. To assess the single-channel permeability of Cx36 GJs to fluorescent dyes, we combined dye transfer studies with g_j measurements in HeLaCx36-EGFP cell pairs. Typically, we selected cell pairs exhibiting at least one junctional plaque (see Fig. 2a), which usually yields electrical cell–cell coupling; and g_j was higher at larger junctional plaques. Dyes used include (molecular mass of the fluorescent ion, valence): LY (443, −2), Alexa fluor-350 (AFl-350; 326, −1), EAM-1 (MW 266, +1) and EAM-2 (MW 310, +1), ethidium bromide (EtBr; 314, +1) and DAPI (279, +2). Usually, positively charged dyes bind to nucleotides, and due to this binding, the quantum efficiency of their fluorescence increases substantially. Only one class of compounds that generally remains unbound in the cytoplasm, [2-(4-nitro-2,1,3-ben-zoxadiazol-7-

yl)aminoethyl]trimethylammonium (NBD-TMA$^+$), designed originally as a probe for monitoring renal transport of organic cations, has been reported (Bednarczyk et al. 2000). Furthermore, NBD-TMA$^+$ has been used by Burt and colleagues to measure the cationic permeability of GJs formed of different Cx isoforms (Ek-Vitorin and Burt 2005; Ek-Vitorin et al. 2006; Heyman and Burt 2008). They showed that NBD-TMA$^+$ fluorescence intensity is linearly proportional to its concentration. Iodide and bromide salts of NBD-TMA are known as EAM-1 and EAM-2, respectively; their molecular formulas are shown in Fig. 1b. To test whether EAM-1 and EAM-2 bind to cytoplasmic constituents, we pemeabilized cells loaded with EAM dyes by applying>200-mV pulses to the patch pipette or exposing cells to alcohol. We observed a decay of fluorescence approaching zero over a several minutes, which indicates that EAM dyes do not bind to cytoplasmic constituents or do so at low levels.

To measure permeability, pipette 1 filled with dye was attached to cell 1 and pipette 2 without dye was attached to cell 2 (Figs. 1, 2). After opening patch-1, dye diffused to cell 1, followed by dye transfer to cell 2. Typically, fluorescence intensity in cell 1 approached steady state during several minutes, but this time was longer at higher dye transfer rates to cell 2. Approximately 5 min later, the patch in cell 2 was open to measure g_j in a dual whole-cell voltage-clamp mode. The total junctional permeability, P_j, was evaluated using equation 3, which accounted for fluorescence intensity changes in cell 1 (FI_1) and cell 2 (FI_2). The single-channel permeability (P_γ) can be found by dividing P_j by the number of open channels ($n = g_j/\gamma_o$, where γ_o is the open single-channel conductance) at a given time as follows:

$$P_\gamma = \frac{P_j}{g_j/\gamma_o} = \frac{(vol_2 \cdot \Delta FI_2/\Delta t)\,\gamma_o}{(FI_1 - FI_2)\,g_j} \quad (4)$$

Our initial studies revealed that Cx36-expressing cells are permeable to neurobiotin but not to LY and DAPI (Teubner et al. 2000). All these studies were performed using whole-field excitation, which has strong limitations in cells expressing low coupling. The emission light of cell 1 as well as of pipette 1 loaded with dye is relatively intense, and its scattering from cell 2 and surroundings can even exceed the emission light of dye transferred to cell 2 severalfold if the number of operating GJ channels is small and/or channel permeability is low (see Fig. 1a, left). It is assumed that this applies to Cx36 because it exhibits very low single-channel conductance and <1 % of Cx36 GJ channels are functional (F. F. B. unpublished data). To overcome this problem, we used dual excitation, as described earlier (Rackauskas et al. 2007b; Palacios-Prado et al. 2009). In brief, cells were exposed periodically (every 6–9 s in time-lapse mode) to whole-field excitation (see Fig. 1a, left), followed by exposure only of cell 2 to a focused light with diameter of ~15 µm (see Fig. 1a, right). The diameter and intensity of focused light were variable, when necessary. The 3-D micromanipulator was used to change the focus and position of the focused light. To assess P_j, we measured changes in FI_1 during whole-field excitation and in FI_2 during focused excitation. To calibrate emission signals obtained during whole-field and focused excitations, cell 1 was exposed to focused light several times during the experiment. A dual-mode excitation increased the resolution of dye transfer measurements at least 100-fold and allowed us to measure dye transfer even in the presence of few GJ channels.

Permeability of Cx36 GJs to Negatively Charged Dyes

Experiments were performed in a HeLaCx36-EGFP cell pair exhibiting one or several junctional plaque (Fig. 2a). Figure 2c shows that after opening the patch in pipette 1 filled with LY (first arrow), FI_1 started to rise, reaching steady state after ~3.5 min. Fluorescence images measured during whole-field excitation (Fig. 2b) did not show detectable LY transfer

into cell 2, while the FI_2 trace measured during the focal excitation demonstrates the FI_2 rise, reaching approximately 0.3 % of the FI_1 value at ~320 s (FI_2 trace in Fig. 2c). After opening the patch into cell 2 (second arrow), we applied repeated (1.5 s) voltage ramps, changing during 1 s from −10 to +10 mV to cell 1, to measure I_j, which allowed us to find that $g_j = 6.4$ nS. FI_2 started to decay after opening the patch into cell 2, indicating LY flux from cell 2 to pipette 2. The bottom trace shows P_γ calculated using equation 4. Data points positioned inside the gray rectangle resulted in $P_\gamma = 0.0618 \pm 0.0024 \times 10^{-15}$ cm/s ($n = 26$). On average $P_{\gamma,LY} = 0.068 \pm 0.012 \times 10^{-15}$ cm^3/s ($n = 14$). Using AFl-350 instead of LY, we found similar dynamics of FI_1 and FI_2, but on average $P_{\gamma,AFl\text{-}350}$ was fourfold higher: $P_{\gamma,AFl\text{-}350} = 0.27 \pm 0.06 \times 10^{-15}$ cm^3/s ($n = 11$). Fluorescence images obtained using a whole field were similar to the one shown in Fig. 2b; i.e., AFl-350 transfer signals were comparable with background fluorescence. In summary, the data show that on average $P_{\gamma,LY}$ is approximately fourfold smaller than $P_{\gamma,AFl\text{-}350}$, which could be mainly due to two negative charges instead of one. Figure 2c, d shows that P_γ values remained constant during their evaluation period, which indicates that during the experiment lasting ~5 min, there was no substantial dye bleaching or dye binding to cytoplasmic constituents.

In evaluations of P_γ, the number of GJ channels was calculated assuming that $\gamma_o = 15$ pS (Teubner et al. 2000), which can be even smaller, between 10 and 15 pS (Srinivas et al. 1999). Furthermore, measured g_j is defined by channels that can be only at the main open state but not at the residual state, which is not permeable to dyes and metabolites even in Cxs with significantly higher γ_os, such as Cx43 and Cx46 (Qu and Dahl 2002; Bukauskas et al. 2002a). There are no reports that reliably demonstrate gating of Cx36 GJ channels to the residual state, which is an indication of the *fast* gate. In addition, g_j measurements were performed at small V_js (~10 mV) that cannot induce gating in Cx36 exhibiting exceptionally low sensitivity to V_j (Srinivas et al. 1999; Teubner et al. 2000). To further exploit this aspect, we examined g_j – V_j dependence in HeLaCx36-EGFP cell pairs in response to a slow V_j change from 0 to +100 and −100 mV (Fig. 3a). An averaged ($n = 9$) and normalized g_j – V_j plot is shown as a black solid line in Fig. 3b. The white line is a fitting curve obtained using a stochastic four-state model (S4SM) (Paulauskas et al. 2009; see function of the model online: http://connexons.aecom.yu.edu/Applet.htm). During simulation, we assumed that Cx36 GJs contain two *slow* gates, operating between open and closed states with conductances of 15 and 0 pS, respectively. We used an Exkor algorithm of global optimization to fit an experimental g_j – V_j plot (see movies at http://connexons.aecom.yu.edu/Research.htm, illustrating performance of global optimization) that allowed us to evaluate parameters of the gates and consequently changes of open probability of the A and B hemichannels, $P_{H,A}$ and $P_{H,B}$, depending on V_j (Fig. 3c). The summarized g_j – V_j plot is slightly asymmetric, which is reflected in a small asymmetry of $P_{H,A}$ – V_j and $P_{H,B}$ – V_j plots. At $V_j = 0$, $P_{H,A} = 0.85$ and $P_{H,B} = 0.88$, and consequently the open probability of GJs is 0.75 (0.85×0.88). Therefore, under control/normal conditions, ~75 % of functional Cx36 GJs are open at any given time. It is typical for many Cxs to be gated under resting ($V_j = 0$ mV) conditions (Bukauskas et al. 2002b; Palacios-Prado et al. 2009, 2010). If GJs are indeed gated by the slow gate, then evaluations of P_γ would be in accordance with equation 4. If a fraction of channels could be gated to the residual state by the *fast* gate, then P_γ could be slightly underevaluated because at the same g_j a smaller number of channels would be in the fully open state.

Permeability of Cx36 GJs to Positively Charged Dyes

To study permeability to cationic dyes, we used EAM-1 and EAM-2 as well as EtBr and DAPI. Figure 2d shows the dynamics of FI_1 and FI_2 of EAM-2 fluorescence in a He-LaCx36-EGFP cell pair with $g_j = 5$ nS, which corresponds to ~333 channels (5 nS/15 pS). Arrows indicate patch openings in cell 1 and cell 2. The bottom trace shows the calculated

values of P_γ. Averaged P_γ values of EAM-1 and EAM-2 are alike ($2.31 \pm 0.562 \times 10^{-15}$ cm^3/s [$n = 9$] and $2.10 \pm 0.67 \times 10^{-15}$ cm^3/s [$n = 9$], respectively), presumably due to a similarity in their structure and the net charge (+1), while a small difference in their MW (266 vs. 310) may explain why $P_{\gamma,EAM\text{-}1}$ is slightly higher than $P_{\gamma EAM\text{-}2}$. Thus, the P_γs of EAM-1 and EAM-2 are ~ 10-fold higher than the P_γ of AFl-350, which is of approximately the same molecular mass. The polarity of the net charge should be a major reason for this difference. Movies 1 and 2 in the supplements show a barely detectable transfer of EAM-1 when only whole-field excitation was used (Movie 1), and it was significantly more expressed using a dual-excitation mode (Movie 2) in the cell pair exhibiting g_j of 4.3 nS. To compare the cationic permeability of Cx36 with other Cxs using the same technique, we examined P_γ for EAM-1 in HeLa cells expressing Cx43-EGFP and found that $P_{\gamma,EAL\text{-}1} = 42 \pm 8\ 9\ 10^{-15}$ cm^3/s ($n = 6$), which is between $P_{\gamma,LY}$ and $P_{\gamma,AFl\text{-}350}$ reported by us earlier (Rackauskas et al. 2007b). Thus, Cx43 GJs in general are not charge-selective, in harmony with earlier reports (Verselis et al. 2000; Heyman and Burt 2008; Kanaporis et al. 2011).

When cell 1 of a Cx36–EGFP cell pair was loaded with EtBr$^+$ or DAPI^{2+}, we initially observed increasingly strong fluorescence labeling of the nucleus of cell 1 and, with some delay, labeling of the nucleus of cell 2. When only whole-field excitation was used for EtBr or DAPI transfer, it was barely detectable. Labeling of cell 2 was significantly more expressed using a dual-excitation mode (see Movies 3 and 4 for EtBr transfer in supplemental materials). Typically, we observed the spread of the wave across the nucleus starting from the position where pipette 1 is located and in cell 2 starting from the side of the nucleus that was closer to the junction (Fig. 4b and Movies 5 and 6 in supplemental materials).

Figure 4c, d shows FI_1 and FI_2 changes of EtBr and DAPI after opening the patch in cell 1. FI_2 started to rise only after fluorescence intensities of EtBr or DAPI in cell 1 almost reached the steady-state level. During the initial period after patch opening in cell 1, EtBr or DAPI quickly bound to DNA, resulting in a very low free concentration. After saturation of binding to nucleotides, the free concentration of EtBr and DAPI increased, allowing to observe a fluorescence rise in cell 2 (Fig. 3c, d). After transferring cell 2 into a whole-cell voltage-clamp configuration, there were no signs of decay in FI_2, which was well defined in Fig. 2c, d. This may be due to the fact that most of the fluorescence comes from bound dyes, while unbound EtBr or DAPI exhibit very low fluorescence. All examined cell pairs exhibited weak but detectable cell-to-cell transfer of EtBr ($n = 11$) and DAPI ($n = 13$) using whole-field excitation, as seen in Fig. 4a, b, which typically was not achievable for LY and AFl-350. Due to strong binding of EtBr and DAPI to DNA, quantification of P_γs using equation 4 is not possible. These data support the conclusion that permeability of Cx36 channels is significantly higher for positively than negatively charged dyes. This is also supported by an earlier report (Teubner et al. 2000) showing a transfer of positively charged neurobiotin but no transfer of LY from HeLaCx36 cells injected with dye to the first-order neighboring cells. At this time, we did not use a dual-mode excitation to study dye transfer.

Permeability of the single Cx36-EGFP GJ channel for anionic and cationic dyes is summarized in Table 1 and Fig. 5a. Thus, Cx36 GJ channels exhibit strong cationic selectivity, similar to Cx40 (Heyman et al. 2009), but with ~100-fold smaller in absolute values of P_γs.

Discussion

Cx36 is expressed preferentially in neurons and β-cells of the pancreas in adults (Condorelli et al. 1998; Serre-Beinier et al. 2000), while its expression could be even broader during embryonic stages and in neonatals (Dobrenis et al. 2005). It was shown, by following the

diffusion of micro-injected dyes in primary β-cells, that Cx36 GJs are more permeable to positively than negatively charged tracers (Charpantier et al. 2007). Cell-to-cell transfer of dyes depends also on the number of open GJ channels which can be estimated from g_j measurements. One of the key parameters allowing comparison of the permeability of GJ channels formed of different Cx isoforms is single-channel permeability, P_γ. Here, we combined imaging and electrophysiological methods to estimate P_γs for dyes differing in molecular mass and net charge. Many of the fluorescent dyes used resemble, based on size and charge, numerous vital metabolites, which are not fluorescent and whose permeability cannot be measured directly.

Cell-to-cell transfer of atomic ions and metabolites depends also on ionophoresis by V_j, which can accelerate or decelerate the motion of charged molecules in the GJ channel pore (Palacios-Prado and Bukauskas 2012). Thus, metabolic cell–cell communication depends on the permeability of GJs, their number and V_j. We evaluated P_γ before the patch in cell 2 was open, i.e., at $V_j = 0$ mV, thereby preventing dye leak into pipette 2. If the patch of pipette 2 is open during dye transfer measurements, then the following equation for permeability evaluation (Palacios-Prado and Bukauskas 2009) should be used:

$$P_{j,V_{j=0}} = \frac{\left[vol_2 \cdot (\Delta FI_2 / \Delta t) + P_P FI_2\right]}{\left[FI_1 - FI_2\right]} \quad (5)$$

where P_p is a constant characterizing dye diffusion from cell 2 to pipette 2, which can be considered as infinite volume. FI_2 decay after patch opening in cell 2 can be seen in Fig. 2c, d. From that moment, equation 5 should be used to evaluate P_j. Typically, we measured the kinetics of FI_2 decay under rapid chemical uncoupling (heptanol, CO_2, etc.) for P_p estimation. Then, $P_{j,V_{j=0}} = 0$ and equation 5 can be transformed as follows: $P_p = -$ vol$_2 \cdot (\Delta FI_2 / \Delta t) / FI_2$ and used to estimate P_p. If dye transfer is performed under the influence of transjunctional voltage, then equation 6 (Palacios-Prado and Bukauskas 2009), derived from the GHK formalism (Hille 2001), should be used:

$$P_j = \frac{\left[(vol_2 \Delta FI_2 / \Delta t) + P_P FI_2\right]\left[1 - \exp\left(-zFV_j / RT\right)\right]}{\left(zFV_j / RT\right)\left[FI_1 - FI_2 \exp\left(-zFV_j / RT\right)\right]} \quad (6)$$

where z is the net charge of the dye molecule, F is Faraday's constant, R is the gas constant and T is the absolute temperature. We used this equation in correlative studies of g_j and permeability modulation by V_j in heterotypic Cx43/Cx45 GJs and in separating ionophoretic and diffusional components in dye transfer (Palacios-Prado and Bukauskas 2009). In neurons, cardiomyocytes and other excitable cells, V_j can reach ~100 mV during asynchronous action potentials and substantially modulate metabolic cell–cell commination. Smaller but long-lasting values of V_js could be due to differences in the resting potential, which typically is small under normal/control conditions and can be substantial in transitional zones between normal and pathological regions.

We found that $P_{\gamma,AFl-350}$ of Cx36 is smaller than those of Cx43, Cx40, Cx45, and Cx57 by approximately 358, 138, 23 and 4 times, respectively, while $P_{\gamma,LY}$ is smaller than those for LY of Cx43, Cx40 and Cx45 for ~361, 101 and 16 times, respectively (Rackauskas et al. 2007b; Palacios-Prado et al. 2009). In contrast, $P_{\gamma,AFl-350}$ of Cx36 is ~6.5-fold higher than that of mCx30.2 (Rackauskas et al. 2007b), which exhibits smaller single-channel conductance (~10 vs. 15 pS [Srinivas et al. 1999; Teubner et al. 2000; Kreuzberg et al. 2005]). P_γ values of EAM-1 and EAM-2 are ~2.2×10^{-15} cm^3/s, which is ~10-fold higher than permeability for anionic dyes AFl-350 and LY. This correlates with transfer of EtBr

and DAPI detectable even using whole-field excitation. All these data are summarized in Table 1 and illustrated in Fig. 5b.

Data collected by different groups generally are in a broad agreement that P_γ decreases with an increase in molecular mass (Heyman and Burt 2008; Weber et al. 2004). The relationship between $P_{\gamma,\text{AFl-350}}$ and $P_{\gamma,\text{LY}}$ of different Cxs and the single-channel conductance (Fig. S1 in supplemental materials) shows that the permeability of GJs is not directly proportional to their unitary conductance. There is a tendency for higher P_γs at higher γ_0s. Thus, the channel pore cannot be viewed as a simple cylinder due to the interaction of charged permeant molecules with charged domains of the pore. This interaction is reflected in a broad variation of charge selectivity from nonselective to highly cationic or even some anionic selectivity (Veenstra et al. 1994a, 1994b; Verselis and Veenstra 2000; Verselis et al. 2000). It was predicted that an important determinant of charge selectivity is located, at least for Cx32 and Cx46, in the E1 domain (Trexler et al. 2000). Most of the recently collected data support a view that GJs preferentially exhibit no or weak anionic selectivity, while only cationic selectivity can be strong (Heyman et al. 2009; Kanaporis et al. 2011).

Previously, using a dual-mode excitation, we reported that $P_{\gamma,\text{AFl-350}}$ and $P_{\gamma,\text{LY}}$ of Cx43 is ~2.6- and 3.6-fold larger than those of Cx40 and ~16- and 22-fold larger than those of Cx45. These ratios differ from those reported by Kanaporis et al. (2011), demonstrating that $P_{\gamma,\text{AFl-350}}$ and $P_{\gamma,\text{LY}}$ of Cx43 are 11- and 6-fold smaller than those reported by Rackauskas et al. (2007b), respectively. Furthermore, Cx40 and Cx45 exhibit similar $P_{\gamma,\text{LY}}$, while in Rackauskas et al. (2007b) $P_{\gamma,\text{LY}}$ of Cx40 is approximately sixfold higher than that in Cx45, which exhibits approximately fivefold smaller single-channel conductance. Furthermore, the reported value for $P_{\gamma,\text{AFl-350}}$ of Cx43 measured using a compartmental model is 180×10^{-15} cm^3/s (Nitsche et al. 2004) and that for $P_{\gamma,\text{LY}}$ measured in HeLa Cx43 transfectants is $\sim 39 \times 10^{-15}$ cm^3/s (Eckert 2006), which are even higher than those in Rackauskas et al. (2007b). Measurements of P_γ are highly complex, and there are several potential sources of error, indicated in Weber et al. (2004) and Eckert (2006). Among them, the most critical are those related to proper measurement of g_j and emitted light of cell 2. A major error in determining g_j is due to a series resistance (Wilders and Jongsma 1992), which can be minimized using low-resistance patch pipettes, and excluding measurements in cell pairs with g_js exceeding ~20 nS. In HeLaCx36-EGFP cell pairs, measured g_j was relatively low, on average ~5 nS. Thus, evaluations of P_γ performed for Cx36 should not be affected substantially by series resistance.

Thus, we demonstrate that Cx36 GJs exhibit strong cationic selectivity, which may explain some unsuccessful attempts to demonstrate LY transfer in between neurons and to some degree reduces existing controversy on this issue. Many signaling molecules and metabolites, such as cAMP, IP$_3$, ATP, ADP, AMP and PCr (phosphocreatine), are charged negatively, which predicts their relatively low permeability rate through Cx36 GJs. At the same time, permeability to cations, including K$^+$, which is a major cell-to-cell charge carrier, should be high, which assumes that Cx36 GJs are specialized more for electrical than for metabolic cell–cell communication. Preferential cationic vs. anionic selectivity among Cx isoforms in which permselectivity was examined rigorously suggest that this conclusion has the potential to be applied to more Cx isoforms.

Supplementary Material

Refer to Web version on PubMed Central for supplementary material.

Acknowledgments

References

Bednarczyk D, Mash EA, Aavula BR, Wright SH. NBD-TMA: a novel fluorescent substrate of the peritubular organic cation transporter of renal proximal tubules. Pflugers Arch. 2000; 440:184–192. [PubMed: 10864014]

Bedner P, Niessen H, Odermatt B, Kretz M, Willecke K, Harz H. Selective permeability of different connexin channels to the second messenger cyclic AMP. J Biol Chem. 2006; 28:6673–6681. [PubMed: 16373337]

Bennett MV, Verselis VK. Biophysics of gap junctions. Semin Cell Biol. 1992; 3:29–47. [PubMed: 1320429]

Bukauskas FF. Inducing de novo formation of gap junction channels. Method Mol Biol. 2001; 154:379–393.

Bukauskas FF, Peracchia C. Two distinct gating mechanisms in gap junction channels: CO_2-sensitive and voltage-sensitive. Biophys J. 1997; 72:2137–2142. [PubMed: 9129815]

Bukauskas FF, Verselis VK. Gap junction channel gating. Biochim Biophys Acta. 2004; 1662:42–60. [PubMed: 15033578]

Bukauskas FF, Weingart R. Voltage-dependent gating of single gap junction channels in an insect cell line. Biophys J. 1994; 67:613–625. [PubMed: 7524710]

Bukauskas FF, Bukauskiene A, Verselis VK. Conductance and permeability of the residual state of connexin43 gap junction channels. J Gen Physiol. 2002a; 119:171–186. [PubMed: 11815667]

Bukauskas FF, Bukauskiene A, Verselis VK, Bennett MVL. Coupling asymmetry of heterotypic connexin 45/connexin 43-EGFP gap junctions: properties of fast and slow gating mechanisms. Proc Natl Acad Sci USA. 2002b; 99:7113–7118. [PubMed: 12011467]

Campbell RE, Ducret E, Porteous R, Liu X, Herde MK, Wellerhaus K, Sonntag S, Willecke K, Herbison AE. Gap junctions between neuronal inputs but not gonadotropin-releasing hormone neurons control estrous cycles in the mouse. Endocrinology. 2011; 152:2290–2301. [PubMed: 21447638]

Charpantier E, Cancela J, Meda P. Beta cells preferentially exchange cationic molecules via connexin 36 gap junction channels. Diabetologia. 2007; 50:2332–2341. [PubMed: 17828386]

Condorelli DF, Parenti R, Spinella F, Salinaro AT, Belluardo N, Cardile V, Cicirata F. Cloning of a new gap junction gene (Cx36) highly expressed in mammalian brain neurons. Eur J Neurosci. 1998; 10(3):1202–1208. [PubMed: 9753189]

Dobrenis K, Chang H, Pina-Benabou MH, Woodroffe A, Lee SC, Rozental R, Spray DC, Scemes E. Human and mouse microglia express connexin36, and functional gap junctions are formed between rodent microglia and neurons. J Neurosci Res. 2005; 82:306–315. [PubMed: 16211561]

Eckert R. Gap-junctional single-channel permeability for fluorescent tracers in mammalian cell cultures. Biophys J. 2006; 91:565–579. [PubMed: 16632504]

Ek-Vitorin JF, Burt JM. Quantification of gap junction selectivity. Am J Physiol Cell Physiol. 2005; 289:C1535–C1546. [PubMed: 16093281]

Ek-Vitorin JF, King TJ, Heyman NS, Lampe PD, Burt JM. Selectivity of connexin 43 channels is regulated through protein kinase C–dependent phosphorylation. Circ Res. 2006; 98:1498–1505. [PubMed: 16709897]

Goldberg GS, Valiunas V, Brink PR. Selective permeability of gap junction channels. Biochim Biophys Acta. 2004; 1662:96–101. [PubMed: 15033581]

Harris AL. Emerging issues of connexin channels: biophysics fills the gap. Q Rev Biophys. 2001; 34:325–427. [PubMed: 11838236]

Harris AL. Connexin channel permeability to cytoplasmic molecules. Prog Biophys Mol Biol. 2007; 94:120–143. [PubMed: 17470375]

Hernandez VH, Bortolozzi M, Pertegato V, Beltramello M, Giarin M, Zaccolo M, Pantano S, Mammano F. Unitary permeability of gap junction channels to second messengers measured by FRET microscopy. Nat Methods. 2007; 4:353–358. [PubMed: 17351620]

Heyman NS, Burt JM. Hindered diffusion through an aqueous pore describes invariant dye selectivity of Cx43 junctions. Biophys J. 2008; 94:840–854. [PubMed: 17921206]

Heyman NS, Kurjiaka DT, Ek-Vitorin JF, Burt JM. Regulation of gap junctional charge selectivity in cells coexpressing connexin 40 and connexin 43. Am J Physiol Heart Circ Physiol. 2009; 297:H450–H459. [PubMed: 19465552]

Hille, B. Ionic channels of excitable membranes. Sinauer Associates; Sunderland: 2001.

Jain R, Lammert E. Cell–cell interactions in the endocrine pancreas. Diabetes Obes Metab. 2009; 11:159–167. [PubMed: 19817798]

Kanaporis G, Brink PR, Valiunas V. Gap junction permeability: selectivity for anionic and cationic probes. Am J Physiol Cell Physiol. 2011; 300:C600–C609. [PubMed: 21148413]

Kreuzberg MM, Sohl G, Kim J, Verselis VK, Willecke K, Bukauskas FF. Functional properties of mouse connexin30.2 expressed in the conduction system of the heart. Circ Res. 2005; 96:1169–1177. [PubMed: 15879306]

Nitsche JM, Chang H, Weber PA, Nicholson BJ. A transient diffusion model yields unitary gap junctional permeabilities from images of cell-to-cell fluorescent dye transfer between *Xenopus* oocytes. Biophys J. 2004; 86:2058–2077. [PubMed: 15041648]

Palacios-Prado N, Bukauskas FF. Heterotypic gap junction channels as voltage-sensitive valves for intercellular signaling. Proc Natl Acad Sci USA. 2009; 106:14855–14860. [PubMed: 19706392]

Palacios-Prado N, Bukauskas FF. Modulation of metabolic communication through gap junction channels by transjunctional voltage; synergistic and antagonistic effects of gating and ionophoresis. Biochim Biophys Acta. 2012; 1818:1884–1894. [PubMed: 21930112]

Palacios-Prado N, Sonntag S, Skeberdis VA, Willecke K, Bukauskas FF. Gating, permselectivity and pH-dependent modulation of channels formed by connexin57, a major connexin of horizontal cells in the mouse retina. J Physiol. 2009; 587:3251–3269. [PubMed: 19433576]

Palacios-Prado N, Briggs SW, Skeberdis VA, Pranevicius M, Bennett MV, Bukauskas FF. pH-dependent modulation of voltage gating in connexin45 homotypic and connexin45/connexin43 heterotypic gap junctions. Proc Natl Acad Sci USA. 2010; 107:9897–9902. [PubMed: 20445098]

Pan F, Paul DL, Bloomfield SA, Völgyi B. Connexin36 is required for gap junctional coupling of most ganglion cell subtypes in the mouse retina. J Comp Neurol. 2010; 518:911–927. [PubMed: 20058323]

Peracchia C. Chemical gating of gap junction channels; roles of calcium, pH and calmodulin. Biochim Biophys Acta. 2004; 1662:61–80. [PubMed: 15033579]

Pereda AE, Bell TD, Faber DS. Retrograde synaptic communication via gap junctions coupling auditory afferents to the Mauthner cell. J Neurosci. 1995; 15:5943–5955. [PubMed: 7666179]

Pereda A, O'Brien J, Nagy JI, Bukauskas F, Davidson KG, Kamasawa N, Yasumura T, Rash JE. Connexin35 mediates electrical transmission at mixed synapses on Mauthner cells. J Neurosci. 2003; 23:7489–7503. [PubMed: 12930787]

Ponsioen B, van Zeijl L, Moolenaar WH, Jalink K. Direct measurement of cyclic AMP diffusion and signaling through connexin43 gap junctional channels. Exp Cell Res. 2007; 313:415–423. [PubMed: 17150212]

Qu Y, Dahl G. Function of the voltage gate of gap junction channels: selective exclusion of molecules. Proc Natl Acad Sci USA. 2002; 99:697–702. [PubMed: 11805325]

Rackauskas M, Kreuzberg MM, Pranevicius M, Willecke K, Verselis VK, Bukauskas FF. Gating properties of heterotypic gap junction channels formed of connexins 40, 43 and 45. Biophys J. 2007a; 92:1952–1965. [PubMed: 17189315]

Rackauskas M, Verselis VK, Bukauskas FF. Permeability of homotypic and heterotypic gap junction channels formed of cardiac connexins mCx30.2, Cx40, Cx43, and Cx45. Am J Physiol Heart Circ Physiol. 2007b; 293(3):H1729–H1736. [PubMed: 17557922]

Serre-Beinier V, Le Gurun S, Belluardo N, Trovato-Salinaro A, Charollais A, Haefliger JA, Condorelli DF, Meda P. Cx36 preferentially connects beta-cells within pancreatic islets. Diabetes. 2000; 49(5):727–734. [PubMed: 10905480]

Srinivas M, Rozental R, Kojima T, Dermietzel R, Mehler M, Condorelli DF, Kessler JA, Spray DC. Functional properties of channels formed by the neuronal gap junction protein connexin36. J Neurosci. 1999; 19:9848–9855. [PubMed: 10559394]

Teubner B, Degen J, Sohl G, Guldenagel M, Bukauskas FF, Trexler EB, Verselis VK, De Zeeuw CI, Lee CG, Kozak CA, Petrasch-Parwez E, Dermietzel R, Willecke K. Functional expression of the murine connexin36 gene coding for a neuron-specific gap junctional protein. J Membr Biol. 2000; 176:249–262. [PubMed: 10931976]

Trexler EB, Bennett MV, Bargiello TA, Verselis VK. Voltage gating and permeation in a gap junction hemichannel. Proc Natl Acad Sci USA. 1996; 93:5836–5841. [PubMed: 8650179]

Trexler EB, Bukauskas FF, Bennett MVL, Bargiello TA, Verselis VK. Rapid and direct effects of pH on connexins revealed by the connexin46 hemichannel preparation. J Gen Physiol. 1999; 113:721–742. [PubMed: 10228184]

Trexler EB, Bukauskas FF, Kronengold J, Bargiello TA, Verselis VK. The first extracellular loop domain is a major determinant of charge selectivity in connexin46 channels. Biophys J. 2000; 79:3036–3051. [PubMed: 11106610]

Veenstra RD, Wang HZ, Beyer EC, Brink PR. Selective dye and ionic permeability of gap junction channels formed by connexin45. Circ Res. 1994a; 75:483–490. [PubMed: 7520372]

Veenstra RD, Wang HZ, Beyer EC, Ramanan SV, Brink PR. Connexin37 forms high conductance gap junction channels with subconductance state activity and selective dye and ionic permeabilities. Biophys J. 1994b; 66:1915–1928. [PubMed: 7521227]

Veenstra RD, Wang HZ, Beblo DA, Chilton MG, Harris AL, Beyer EC, Brink PR. Selectivity of connexin-specific gap junctions does not correlate with channel conductance. Circ Res. 1995; 77:1156–1165. [PubMed: 7586229]

Verselis, VK.; Veenstra, RD. Gap junction channels. Permeability and voltage gating. In: Hertzberg, E., editor. Advances in molecular and cell biology. Vol. 30. JAI Press; Greenwich: 2000. p. 129-192.

Verselis V, White RL, Spray DC, Bennett MV. Gap junctional conductance and permeability are linearly related. Science. 1986; 234:461–464. [PubMed: 3489990]

Verselis VK, Trexler EB, Bukauskas FF. Connexin hemichannels and cell–cell channels: comparison of properties. Braz J Med Biol Res. 2000; 33:379–389. [PubMed: 10775302]

Weber PA, Chang H, Spaeth KE, Nitsche JM, Nicholson BJ. The permeability of gap junction channels to probes of different size is dependent on connexin composition and permeant-pore affinities. Biophys J. 2004; 87:958–973. [PubMed: 15298902]

Wilders R, Jongsma HJ. Limitations of the dual voltage clamp method in assaying conductance and kinetics of gap junction channels. Biophys J. 1992; 63:942–953. [PubMed: 1384745]
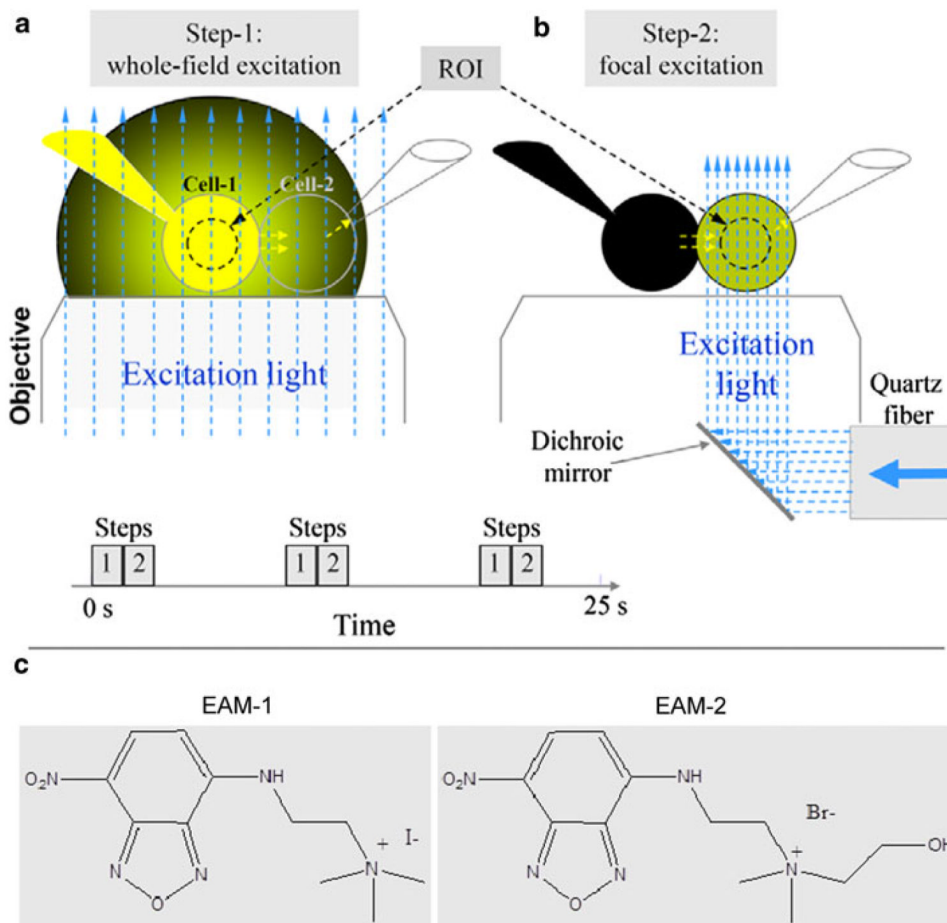
Fig. 1.
Schematics of time-lapse imaging using a dual-fluorescence excitation mode. **a** Whole-field excitation (*vertical, blue, dashed arrows*) of the cell pair with two patch pipettes. Emitted light of dye (*yellow*) in the pipette, and cell 1 creates a large background of scattered light around the cell pair. **b** The same as in **a** but excitation light is focused only to cell 2. This eliminates excitation of dye in cell 1 and the pipette attached to it. **c** Molecular formulas of positively charged fluorescent dyes, EAM-1 and EAM-2
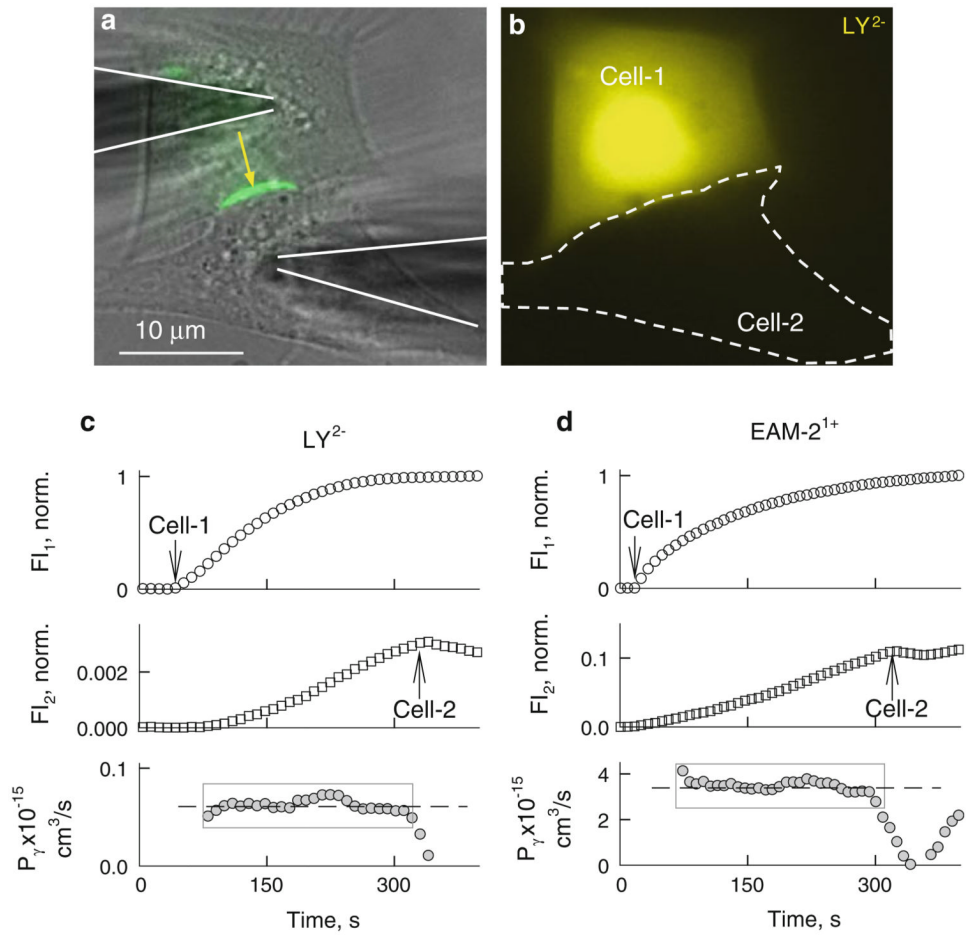
Fig. 2.
Permeability of Cx36-EGFP GJ channels. **a, b** Images of HeLaCx36-EGFP cell pair. **a** Overlapped phase contrast (*gray*) and EGFP (*green*) images; shadows of two patch pipettes are accentuated by continuous lines, and the *yellow arrow* shows the position of the junctional plaque. **b** Fluorescent image of LY obtained using whole-field excitation 5 min after the patch was open to cell 1. There was no detectable LY signal in cell 2; cells were electrically coupled, g_j = 5 nS. **c, d** Examples of time course of changes in LY (**c**) and EAM-2 (**d**) fluorescence in cell 1 (FI_1) and cell 2 (FI_2) and in single-channel permeability (P_γ). *Arrows* point to the moments of patch opening in cell 1 and cell 2
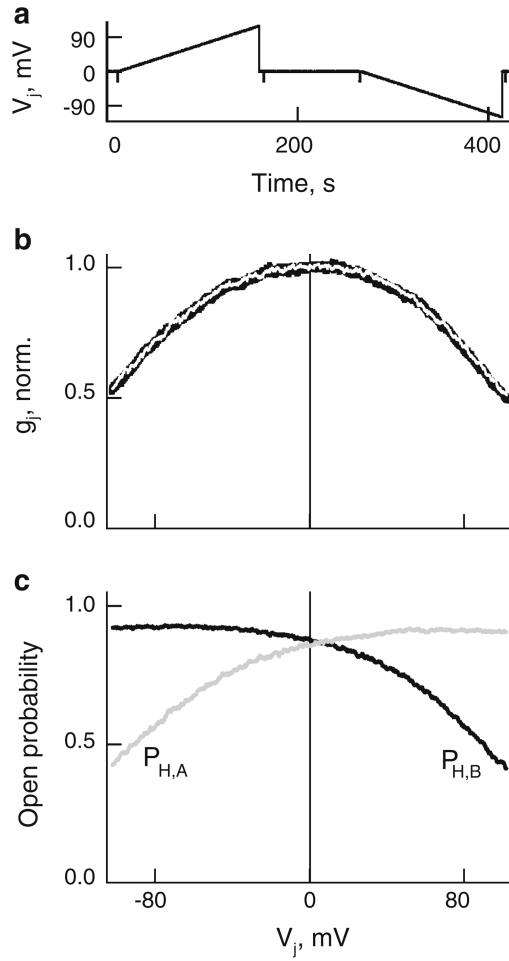
Fig. 3.
Voltage gating of HeLaCx36-EGFP GJs. **a, b** Averaged and normalized g_j – V_j plot (*black solid line* in **b**) obtained in response to V_j ramps (shown in **a**). *White line* is a fitting curve obtained using a S4SM and global optimization. **c** Dependencies of open probabilities of A ($P_{H,A}$) and B ($P_{H,B}$) hemichannels on V_j derived from the S4SM
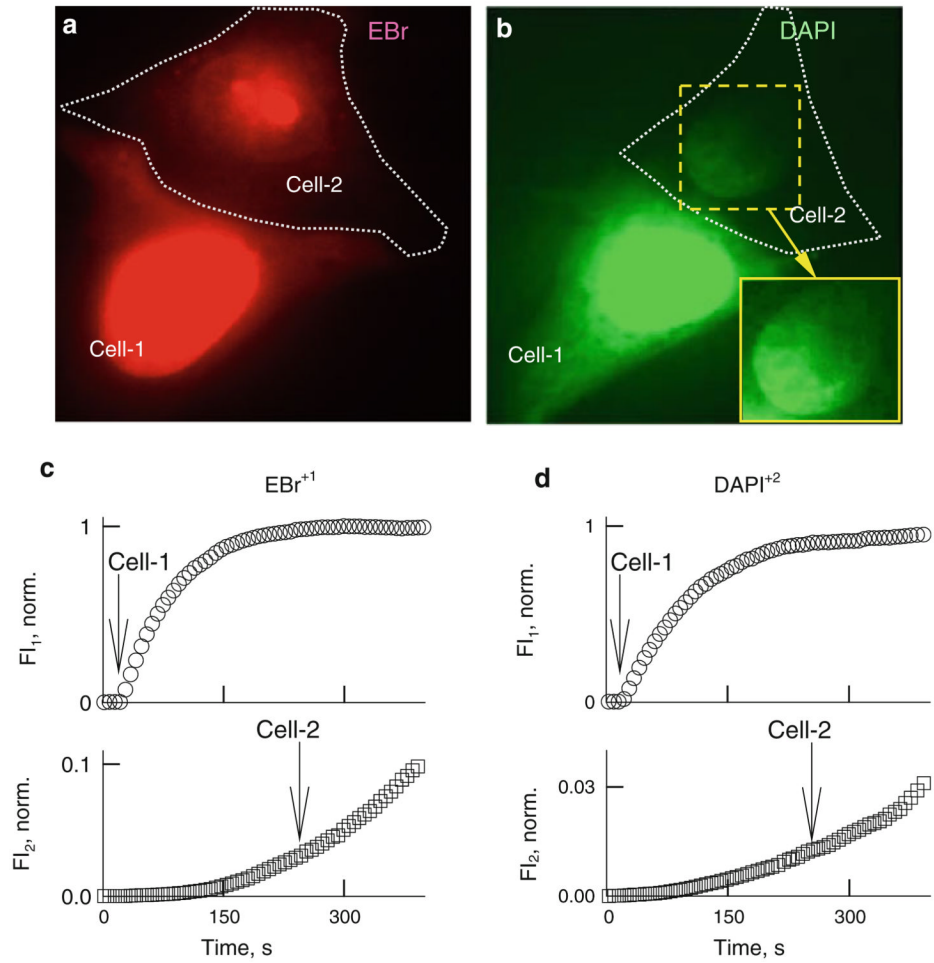
Fig. 4.
Permeability of Cx36– EGFP GJ channels to EtBr and DAPI. Representative images of HeLaCx36-EGFP cell pairs showing transfer of EtBr (**a**) and DAPI (**b**) recorded using whole-field excitation. Enhanced view of nucleus in cell 2 (*inset* in **b**) shows a gradient of fluorescence with higher intensity on the junctional side. Examples of time course of changes in EtBr (**c**) and DAPI (**d**) fluorescence in cell 1 (FI_1) and cell 2 (FI_2). *Arrows* point to the moments of patch opening in cell 1 and cell 2
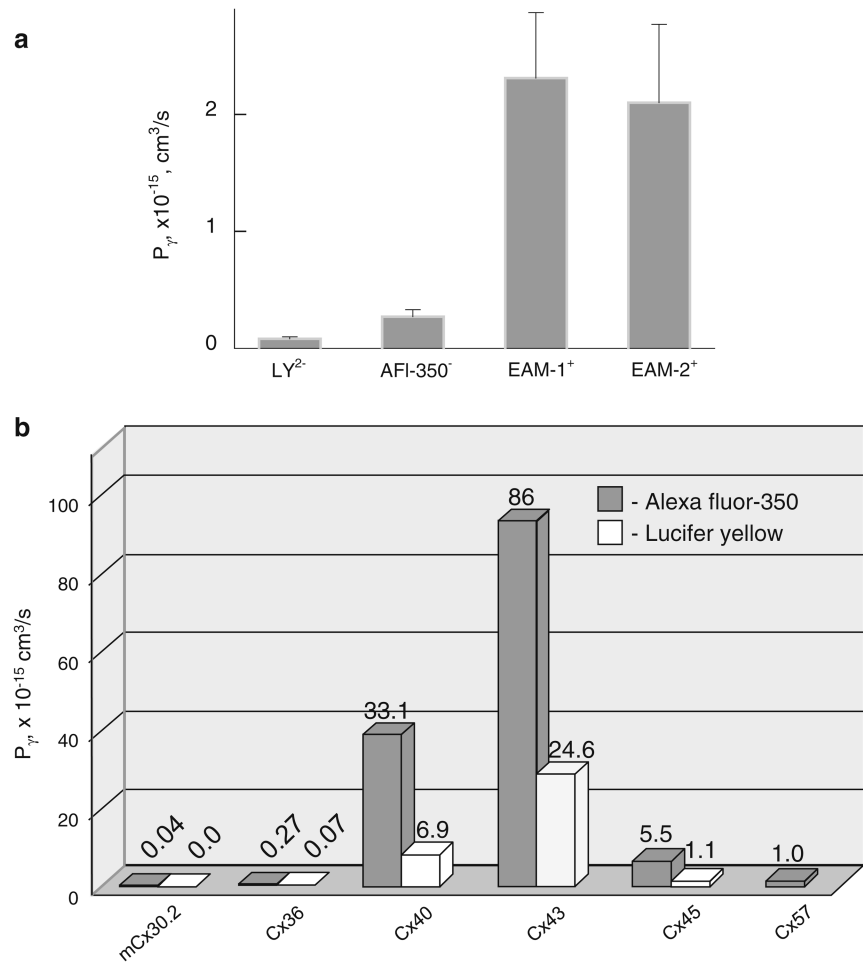
a

b

Fig. 5.
a Averaged single-channel permeability of homotypic Cx36–EGFP GJs for different dyes. **b** Single GJ channel permeabilities of different Cxs. Bars show averaged P_γs of GJ channels for AFl-350 (*gray*) and LY (*white*)

Table 1

Summary of single-channel permeability (P_γ) (mean ± SEM × 10^{-15} cm^3/s) of homotypic GJs for different dyes

Dye	mCx30.2	Cx36	Cx40	Cx43	Cx45	Cx57
AFl-350$^-$	0.04 ± 0.02	0.27 ± 0.06	33.1 ± 6.4	86 ± 7.4	5.5 ± 1	0.95 ± 0.09
	$n = 5$	$n = 11$	$n = 8$	$n = 5$	$n = 3$	$n = 5$
LY^{2-}	n.p.	0.068 ± 0.012	6.9 ± 1.4	24.6 ± 2.4	1.1 ± 0.6	n.e.
	$n = 8$	$n = 13$	$n = 7$	$n = 6$	$n = 3$	
EAM-1$^+$		2.31 ± 0.56		42 ± 8		
		($n = 9$)		($n = 6$)		
EAM-2$^+$		2.10 ± 0.67				
		($n = 9$)				

Data for P_γs of mCx30.2, Cx40, Cx43, Cx45 and Cx57 are from Rackauskas et al. (2007b) and Palacios-Prado et al. (2009) *n.p.* nonpermeable, *n.e.* not examined